Structures 68 (2024) 107184

Contents lists available at ScienceDirect

Structures

journal homepage: www.elsevier.com/locate/structures

# Glazed-level dissipative brace incorporation in a gym building

Stefano Sorace [a,*], Nicola Bidoli [a], Gloria Terenzi [b]

[a] Polytechnic Department of Engineering and Architecture, University of Udine, Via delle Scienze 206, 33100 Udine, Italy
[b] Department of Civil and Environmental Engineering, University of Florence, Via S. Marta 3, 50139 Florence, Italy

ARTICLE INFO

*Keywords:*
Reinforced concrete structures
Masonry infills
Ribbon windows
Seismic retrofit
Dissipative braces
Fluid viscous dampers

ABSTRACT

A wide stock of reinforced concrete (RC) gyms and sports halls was built in Italy from 1960s through 1990s with similar architectural characteristics, among which the two-level partition of façades, displaying continuous masonry infills full in contact with the frame structure on the lower level, and glazed ribbon windows on the upper level. A school gym built in 1976, well representative of this stock of edifices, is examined herein with the aim of assessing its seismic performance in current state and proposing a supplemental damping-based retrofit solution capable of providing adequate protection both to the structure and the non-structural elements. The assessment study is carried out via non-linear dynamic analysis, by modelling infills by means of equivalent diagonal struts, and RC members by plastic hinges. The response of the ribbon windows, not expressly simulated in the analysis, is checked in terms of relevant inter-level drift. The results show a significant inelastic response of the infill panels and the RC columns, and very high drifts on the glazed level, resulting in full collapse conditions of the ribbon windows, under a Basic Design Earthquake (BDE)-scaled seismic action. Consequently, a retrofit hypothesis is conceived, based on the installation of a dissipative bracing system incorporating pressurized fluid-viscous devices on the glazed level, and conventional braces on the infilled level. The location of the system implies no architectural intrusion in the interiors or interruption in the usage of the building. The analyses in post-intervention conditions highlight a remarkable response reduction both in terms of drifts and stress states, consistently with the target design objectives. This allows reaching a safe response of structural elements and ribbon windows, and an elastic response of infills, up to the BDE.

## 1. Introduction

Gym buildings with reinforced concrete (RC) frame structure were designed in Italy from 1960s through 1990s with a recurring architectural scheme, characterized by continuous masonry infills full in contact with the frame structure in the lower portion of the façades, to guarantee interior privacy, and stick-built ribbon windows on the upper portion, in order to provide natural lighting and aeration. These characteristics, which are found in gyms and sports halls, workshops, warehouses, archive storage facilities and manufacturing plants built in the period mentioned above, concur to determine a considerable seismic vulnerability of this wide stock of buildings, especially for the ones designed in 1960s-70s, before modern Seismic Standards were released. Like for other building types belonging to the same period, this is a consequence of poor strength and ductility of RC members, as compared to current performance criteria [1–6], and damageability of masonry infills interacting with the frame structure during response to seismic action [7–13]. But the highest vulnerability of buildings with continuous glazed levels is due to the sudden change in lateral stiffness determined by the presence of infills on the lower façade level only. Indeed, this causes an interlevel drift concentration in the glazed façade portions capable of inducing severe damage, and possible collapse [14–20], even under moderate earthquakes.

In view of this, a seismic assessment and retrofit study on an Italian school gym dating to the mid 1970s, well representative of the characteristics of the above-mentioned class of buildings, is presented herein. The time-history finite element analyses supporting the assessment and retrofit design steps are carried out by expressly modelling infills, by means of equivalent diagonal struts, and checking the response of ribbon windows in terms of relevant inter-level drift. Lumped Takeda-type and fiber plastic hinges are adopted to simulate the response of beams and columns, respectively. The results highlight a remarkable inelastic demand on infill panels and RC columns, as well as a drift demand on the ribbon windows capable of causing their collapse, under a seismic action scaled at the Basic Design Earthquake (BDE) level.

Based on this response, a retrofit intervention based on the

* Corresponding author.
*E-mail addresses:* stefano.sorace@uniud.it (S. Sorace), nicola.bidoli@spes.uniud.it (N. Bidoli), gloria.terenzi@unifi.it (G. Terenzi).

https://doi.org/10.1016/j.istruc.2024.107184
Received 2 April 2024; Received in revised form 12 August 2024; Accepted 26 August 2024

**Fig. 1.** External and internal views of case study building.

installation of a dissipative bracing system is proposed, along the same retrofit line followed in a recent research work [21], where hysteretic dampers are adopted for the seismic protection of both top glazed and bottom masonry levels of a representative warehouse building. The bracing system designed for the gym building examined here incorporates pressurized fluid-viscous (PFV) dampers on the glazed level. This choice is related to the very high specific damping capacity of PFV dampers [22], as well as to their activation capacity from the early seismic response stages [13,23]. This allows avoiding integrative strengthening measures on the structural members, thus limiting the architectural intrusion and the global cost of the interventions, as highlighted by a variety of applications of dissipative systems incorporating PFV dampers to several different types of structures and infrastructures [23–26]. At the same time, conventional non-dissipative braces are installed on the infilled level in view of the notably lower drift demand induced on it by the presence of the masonry panels. This intervention allows reaching a nearly elastic response of all columns and beams, as well as reducing drift demand on infills and windows below the Immediate Occupancy (IO) and Life Safety (LS)-related limits, respectively.

The following sections offer a description of the case study building, a synthesis of the analyses in current and retrofitted conditions, and details about the sizing process and the technical installation of the protection system.

## 2. Case study building

The case study school gym was built in 1976 in a medium-to-high Italian seismic zone. Its structural design was carried out by referring to the 1971 edition of the Italian Technical Standards [27] and related implementing Decree [28], and the 1975 edition of the Seismic Standards [29]. Consistently with the latter, a horizontal force equal to 0.07 times the sum of gravitational loads (including 33 % of live loads) was applied at the roof level in the equivalent seismic static analysis of the frame structure, for both main directions in plan. On the other hand, no specific ductility-related sizing criteria and details were adopted for RC members, since they were not expressly defined in [29].

External and internal views of the building are displayed in Fig. 1. Drawings of one of its identical side façades and structural plan, including X and Y axes in plan of the reference Cartesian system assumed in the structural analyses, are shown in Fig. 2. As highlighted by this figure, the plan is rectangular, with sides of 24.75 m in longitudinal direction, parallel to X, and 12.6 m in transversal direction, parallel to Y. The roof top and the side façades are 7.45 m and 5.8 m high, respectively. The structure is constituted by 8 identical transversal RC frames of two columns each, numbered C1-C2 through C15-C16 in the plan in Fig. 2, placed at a mutual distance of 3.5 m. The cross sections of beams and columns and relevant reinforcement details, redrawn from the original design documentation, are illustrated in Fig. 3. Columns have a mutual rectangular section with 250 mm long sides along X and 300 mm along Y. The primary (sloping) roof beams have a rectangular section 250 mm wide and 300 mm high, whereas the secondary (longitudinal) beams have 250 × 200 mm×mm section. In longitudinal direction the columns are connected by two continuous rectangular beams, situated on top and at a height of 3.15 m (measured on the bottom beam face), with dimensions of 350 × 400 mm×mm and 350 × 300 mm×mm, respectively. The structure of the sloping roof floor and the horizontal under-roof floor is constituted by RC slabs, 200 mm (roof) and 125 mm (under-roof) thick, respectively. The foundation consists of RC cubic footings, with sides of 900 mm for the four corner columns, and 700 mm for the remaining columns. The footings are connected by RC rectangular curb beams sized 350 × 300 mm×mm, both in X and Y. The ground floor is constituted by a 150 mm thick RC slab cast over the underlying crawl space. The mechanical properties of the structural materials derived from the design documentation and the final structural test reports are as follows: mean cubic compressive strength of concrete equal to 35 MPa; yield stress and limit stress of steel equal to 380 MPa and 532 MPa, respectively.

All infills are made of a double layer of 120 mm-thick solid bricks. The stick-built ribbon windows are made of aluminium frames and annealed glass, and consist of seven panels along both side façades, as determined by the sequence of eight RC columns. Each panel is subdivided into six single tilt windows by aluminium profiles; the perimeter profiles are connected to the lateral sides of the second level columns, the lower side of the top longitudinal beams and the upper side of the intermediate longitudinal beams.

According to the current Italian Technical Standards [30] and relevant Instructions [31], based on the information drawn from the original design documentation, the intermediate "LC2″ knowledge level was achieved for this structure. Consistently, value 1.2 was assumed as "confidence factor", *FC*, i.e. the additional knowledge level-related safety coefficient to be introduced in stress state and displacement related checks.

## 3. Seismic assessment analysis in current state

### 3.1. Finite element model of RC members and infills

The seismic assessment study of the building was carried out, via time-history analysis, by means of the finite element model of the structure displayed in Fig. 4, generated with SAP2000NL calculus

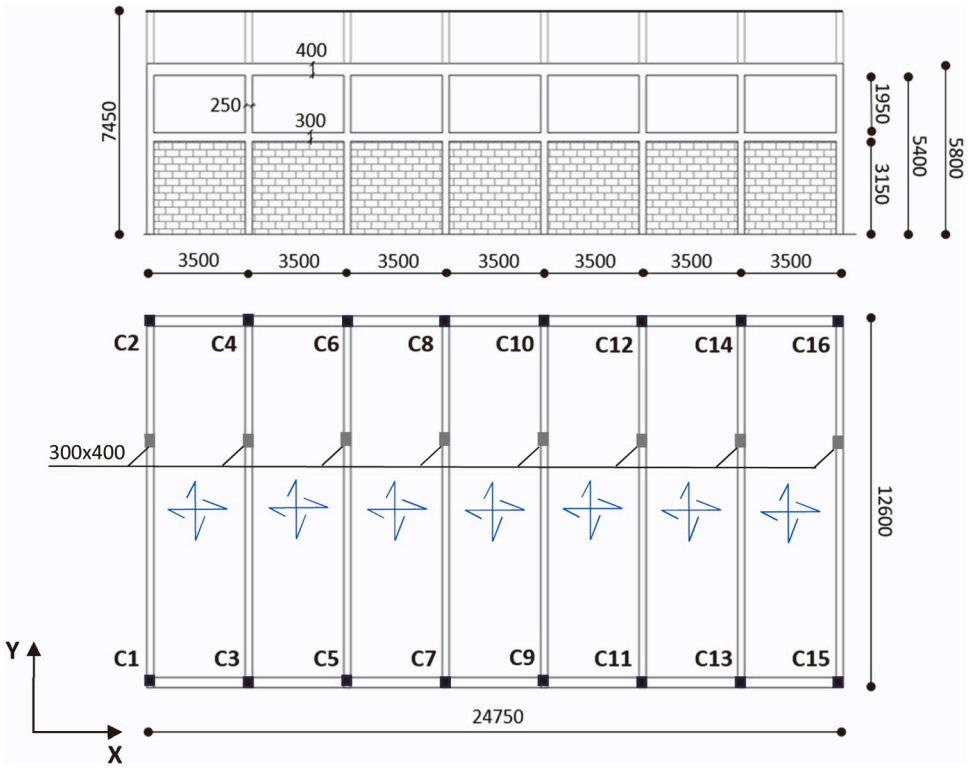


**Fig. 2.** Side façade and structural plan of case study building (dimensions in millimeters).

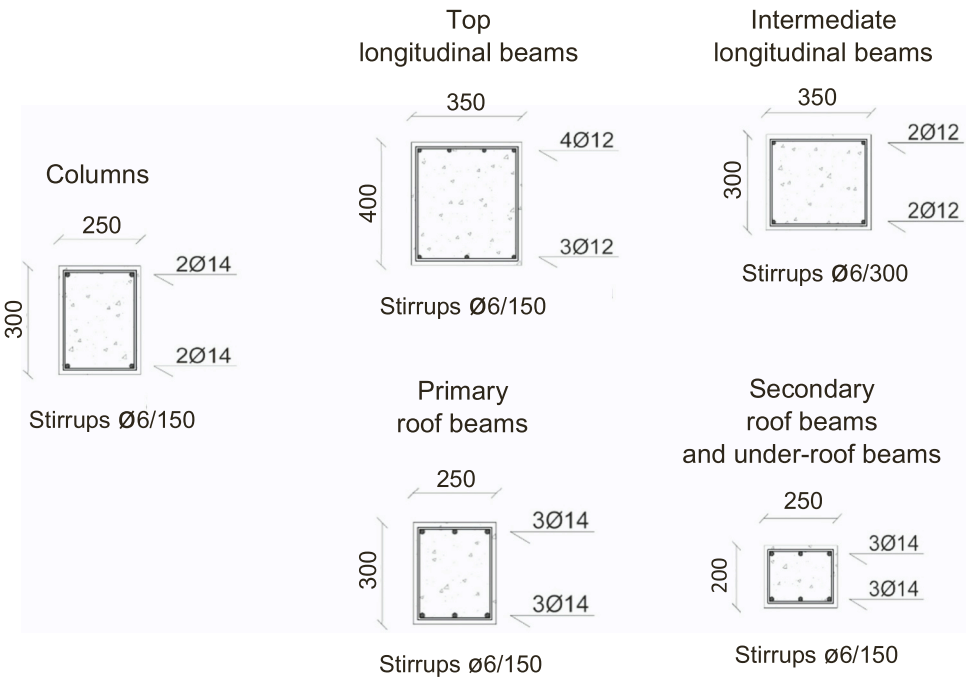


**Fig. 3.** Column and beam cross sections (dimensions in millimeters).

program [32]. Frame-type elements were assumed for columns and beams, and shell elements for the roof and under-roof floor slabs. In order to explore the non-linear response of the structure, lumped plastic hinges were incorporated at the end sections of beams, governed by a Takeda-type hysteretic relationship, and fiber-type plastic hinges—composed of concrete-type and steel-type fibers—at the end sections of columns. Concerning the fiber hinges, which take into account the interaction between axial force and biaxial bending moment, a Mander-type backbone curve associated with a Takeda-type hysteretic model was assigned to the concrete fibers, and a strain hardening elasto-plastic backbone curve with hysteretic kinematic behaviour was assigned to the steel fibers. Like for other commercial finite element structural programs, these hysteretic models are automatically generated in SAP2000NL by introducing the above-mentioned values of the mean cubic compressive strength of concrete, and the yield stress and limit stress of steel.

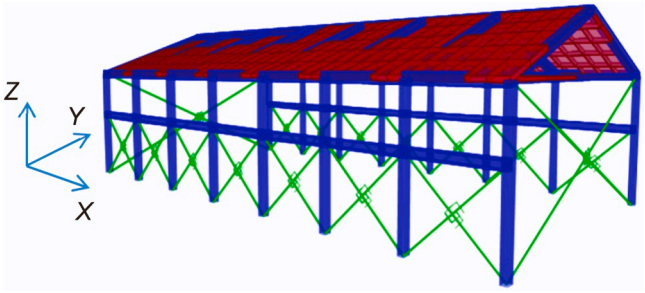


**Fig. 4.** Finite element model of the structure.

Infills were simulated by means of pairs of equivalent crossed compression-only resisting diagonal struts, whose cross section was determined by means of the well-established criteria by Stafford Smith [33] and Bertholdi et al. [34]. The computed axial response of the struts was converted into the lateral force ($H_p$) – drift ($D_p$) response of the panels by basic trigonometric relations. A trilinear $H_p$ – $D_p$ backbone curve was defined in a recent study by the authors' research group [13] to describe the non-linear response of the panels. This curve was subdivided into nine segments, scanned by means of eight $D_p$ performance limit values, calibrated on the response of infills and partitions made of—or including at least a layer of—hollowed bricks. By reassessing the curve for the solid brick-type infills characterizing this case study, the number of segments is reduced to five, displayed by different colours in Fig. 5. In the graph, the backbone curve is traced out in terms of normalized lateral force, $H_{pr}$, i.e. the ratio of $H_p$ to the peak panel force, $H_{p,max}$, and normalized drift, $D_{pr}$, i.e. the ratio of $D_p$ to the panel height $h_p$. $H_{p,max}$ is computed by referring to the minimum stress value associated with the achievement of one of the four possible failure mechanisms of the panel, as defined by the classical relations of Bertholdi et al. [34], recapitulated in [13]. The first response branch (B1, drawn in green) corresponds to a non-cracked elastic behaviour of the panel, whose upper limit can be approximately fixed at a $D_{pr}$ value of 0.05 % [13,35,36]. The corresponding $H_{pr}$ value, which represents the cracking lateral force of the panel, is put as equal to 0.4 [13,37–39]. A first set of diffused hairline fissures starts at the end of B1, causing a loss in lateral stiffness and the start of the cracked response stage. The second segment, named B2 (yellow), is characterized by a growing occurrence of plaster cracks, and the beginning of in-depth cracking effects. The drift ratio threshold can be located at a value of 0.33 %, which is assumed by several Seismic Standards as the limit identifying the Operational (OP) performance level for frame buildings in the presence of interacting masonry infills and partitions (named $D_{pr,OP}$ in the following). Branch B3 (orange) identifies the response stage where the lateral sides of the panel start to detach from the adjacent columns, and the upper side from the top beams, in addition to further cracking. The drift ratio limit of this branch, coinciding with the attainment of the peak response force ($H_{pr}$ = 1), is fixed at 0.5 %, i.e. the value established by most Seismic Standards as the threshold of the Immediate Occupancy performance level (named $D_{pr,IO}$ in the following). The negative slope of the subsequent softening branch can be measured by an angle of about 30° [13,36,38–40]. The first descending segment, B4 (violet), corresponds to the development of damage effects related to the prevailing possible failure mechanism of the panel, with appreciable cracking throughout bricks, local crushing and spalling, as well as sliding in mortar joints. The transition to the second softening branch (B5, red) can be located at a drift ratio of about 0.66 % [13,38–40]. The B5 segment defines a range of severe-to-very severe—and irreparable—damage of panels. The end of B5 segment is fixed at $D_{pr}$ = 1 %; beyond this limit, full in plane damage of panels normally occurs, causing their contribution to the lateral stiffness and strength of an infilled frame building to be nearly annulled. Moreover, since this condition can cause dangers to people's safety, $D_{pr}$ = 1 % can be technically assumed to coincide with the attainment of the Life Safety non-structural performance level. Thus, named $D_{pr,LS}$ the LS-related limit, this is fixed at 1 % in the performance assessment study. The hysteretic behaviour of panels is reproduced by means of a multilinear no-tension pivot-type rule included in SAP2000NL library, as detailed in [13].

The response of the stick-built ribbon windows was assessed by referring to the recommendations of several international Standards, Recommendations and Guidelines about their drift limitations for the IO and LS performance levels [41–45]. These limitations are aimed at preventing: appreciable damage to glazed panels (diffused unsightly cracking and localized corner glass crushing) and aluminium frames (covers detachment from mullion and transom profiles, rubber gasket dislodging, rotations of transom-to-mullion connections)—IO; and failure of windows due to the plasticization of aluminium frames, severe distortion of transom-to-mullion connections, breaking of glass panels and their fall-out—LS. By merging the normative indications according to the evaluation criteria proposed in [16–20], all expressed in terms of window drift ratio, $D_{wr}$, i.e. the ratio of window drift, $D_w$, to window height, $h_w$, substantially converging indications were found about the IO and LS-related limits, named $D_{wr,IO}$ and $D_{wr,LS}$. In particular, the following values resulted from the above-mentioned literature: $D_{wr,IO}$ = 0.5 %, $D_{wr,LS}$ = 1 %, which were assumed as reference values in this study.

The time-history analyses in current state were carried out for the Serviceability Design Earthquake (SDE, with 63 % probability of being exceeded over the reference time period, $V_R$), and the Basic Design Earthquake (BDE, with 10 %/$V_R$ probability) hazard levels assumed by the Italian Standards. The performance in retrofitted conditions was

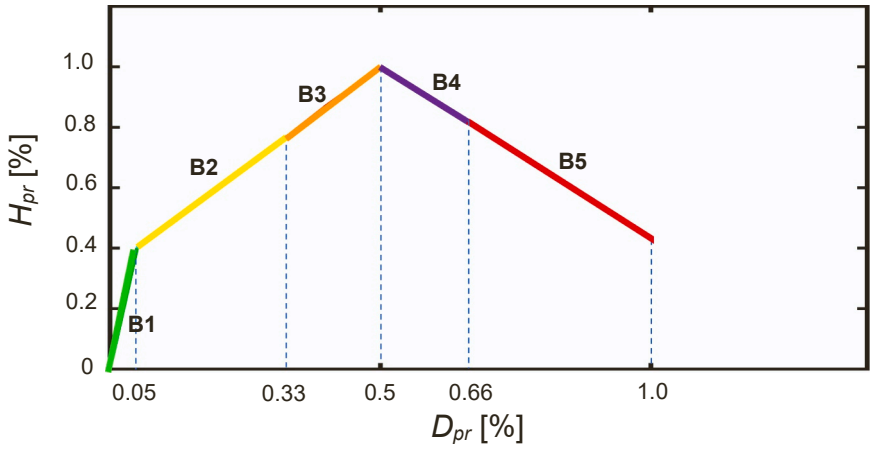


**Fig. 5.** Normalized backbone curve assumed in the analysis of infills.

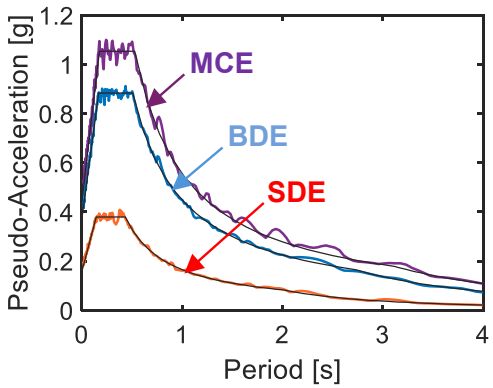


**Fig. 6.** Normative pseudo-acceleration response spectra and median spectra for the seven plus seven generated accelerograms.

examined also at the Maximum Considered Earthquake (MCE, with 5 %/$V_R$ probability), to check the peak displacements of the dampers against their available piston stroke at this maximum normative seismic level, as required by the same Standards. The $V_R$ period was fixed at 75 years, obtained by multiplying the nominal structural life $V_N$ of 50 years by a coefficient of use $C_u$ equal to 1.5, corresponding to the use of the building as a school gym. A set of seven groups of two accelerograms each was applied as input to the time-history analyses. The artificial ground motions were generated from the elastic pseudo-acceleration response spectra at linear viscous damping ratio of 0.05 assumed by [30] for the municipality where the building is located, drawn in Fig. 6. In the figure, the median spectra of the seven plus seven generated ground motions are also plotted. For each group of accelerograms, one of it was applied in X direction, and one in Y.

### 3.2. Results of the analyses

A preliminary modal analysis of the structure highlights a first translational mode along X, with vibration period of 0.364 s and effective modal mass (EMM) equal to 94.9 %; a first translational mode along Y, with period of 0.24 s and EMM of 95.9 %; and a first rotational mode around the vertical axis Z, with period of 0.157 s and EMM of 73.5 %. A second rotational mode, with period of 0.134 s and EMM of 21.2 %, activates a summed EMM of 94.7 % around Z, that is, nearly coinciding with the first-mode EMMs in X and Y.

The results of the time-history analyses at the SDE show that: (a) all structural members are in safe conditions; (b) maximum $D_{pr}$ values equal to 0.06 % are reached for the infills belonging to the side façades, corresponding to the beginning of the B2 segment of the backbone curve, and 0.24 % for the terminal façades, i.e. above the middle of B2; (c) for

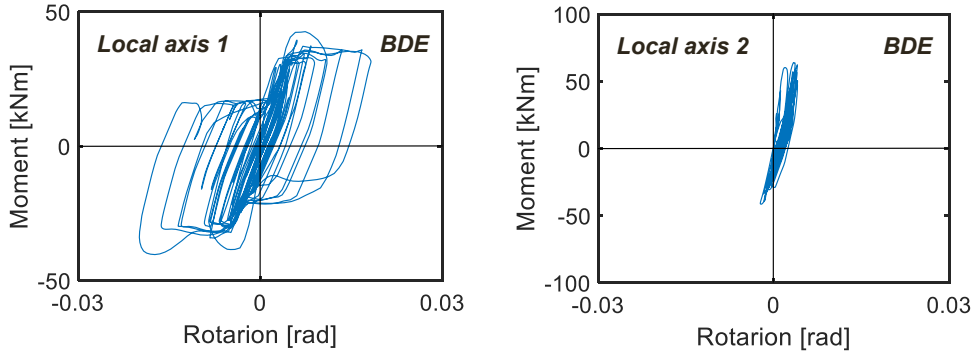


**Fig. 7.** Response cycles of the top plastic fiber hinge of column C1, around its two local axes, obtained from the most demanding BDE-scaled group of input accelerograms.

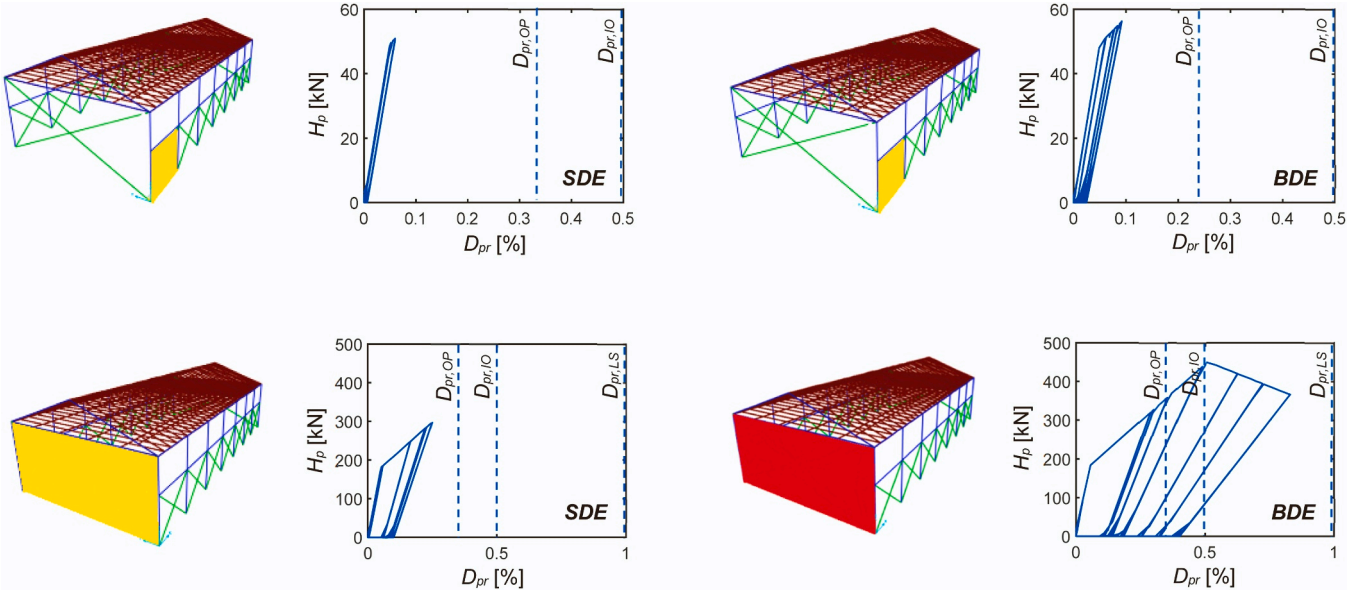


**Fig. 8.** Response cycles of a longitudinal and a transversal infill panel obtained from the most demanding SDE and BDE-scaled groups of input accelerograms, corresponding post-quake states according to the chromatic scale of the backbone curve, and reference $D_{pr,OP}$, $D_{pr,IO}$ and $D_{pr,LS}$ limits.

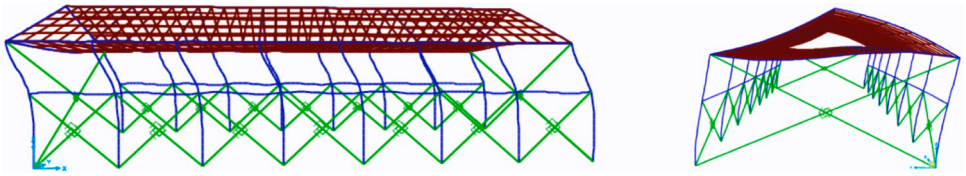

**Fig. 9.** Magnified deformed shapes of the finite element model in X and Y direction.

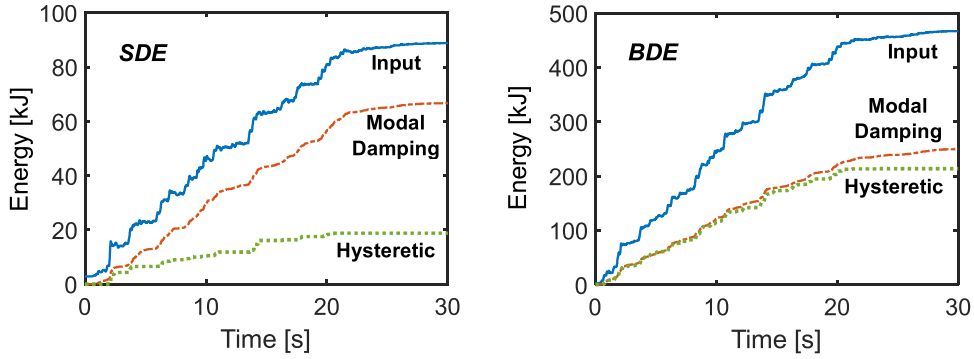


**Fig. 10.** Energy time-histories obtained from the most demanding SDE and BDE-scaled groups of input accelerograms.

the glazed level, peak $D_{wr}$ values equal to 0.88 % are computed, beyond the $D_{wr,IO}$ threshold and slightly lower than $D_{wr,LS}$. The BDE-related performance evaluation highlights that all second level columns are in unsafe conditions, with very similar maximum demand/capacity ratios (due to the regularity and symmetry of the building in plan and elevation), equal to 1.59 in combined axial force/biaxial flexure, and 1.55 in shear. Unsafe stress states are evaluated for the top beams too, with 1.2 demand/capacity ratios in flexure, and 1.09 in shear. Concerning the response of infills, peak $D_{pr}$ values of 0.09 % (early B2 segment portion) are observed for the side façade panels, and 0.79 % (B5), for the terminal façade ones. For windows, maximum $D_{wr}$ values of 2.95 % are achieved, corresponding to full collapse conditions.

By way of example of the results at the BDE, the bending moment-rotation response cycles of the top plastic fiber hinge of column C1 around local axes 1 (parallel to Y) and 2 (parallel to X) are plotted in Fig. 7, and the $H_p - D_{pr}$ response cycles of the infills situated on the C1-C2 and C1-C3 alignments in Fig. 8, for the most demanding of the seven groups of input accelerograms. The $H_p - D_{pr}$ cycles for the same panels at the SDE are visualized in Fig. 8 too. Furthermore, Fig. 9 shows the magnified deformed shape of the finite element model along X, which highlights a remarkable drift demand concentration on the upper level of the structure, caused by the stiffening action of infills on the lower level. This underlines the crucial impact of the latter on the seismic response of the structure and resulting performance evaluations.

The energy response time-histories of the building, plotted in Fig. 10, show 23 %—SDE and 45 %—BDE contributions of the energy dissipated by the hysteretic response of RC members and infills to the total input energy. From the comprehensive viewpoint of energy balance too, this confirms the non-negligible (SDE) and severe (BDE) seismic demand evaluated in terms of drifts and stress states.

## 4. Seismic retrofit design

The data drawn from the assessment study in current conditions, essentially influenced by the sudden lateral stiffness reduction in passing from the infilled to the glazed level of façades, prompt to adopt a supplemental damping-based retrofit solution, instead of conventional ones, like RC member wrapping by FRP fabrics or jacketing, the incorporation of traditional non-dissipative braces or RC shear walls, etc. As mentioned in the Introduction, the adopted strategy consists in the installation of inverse-chevron shaped braces equipped with PFV spring-dampers on the upper level of the frame structure. This choice is aimed at substantially reducing, at this level, both the drift demand on the ribbon windows—causing their severe damage at the SDE and collapse at the BDE—and the significant plastic demand on the RC members at the BDE. In view of the relatively low drift demand on the infills, the

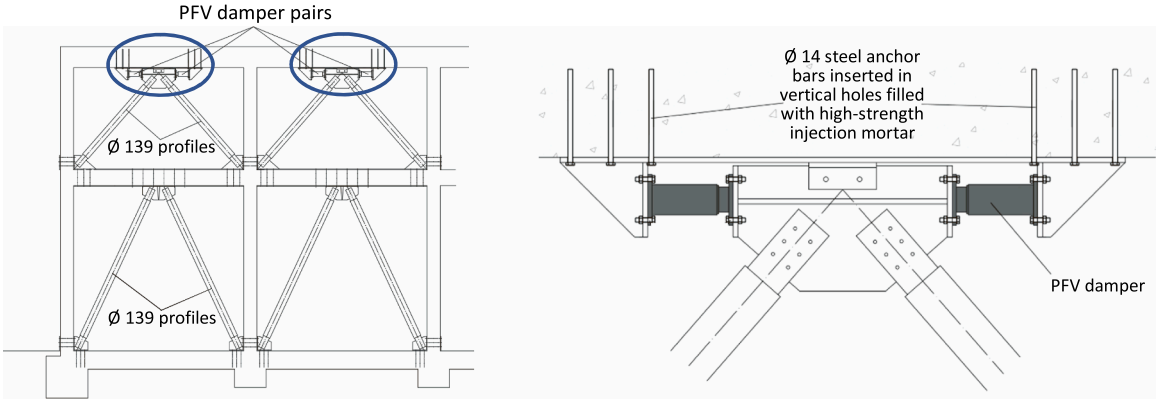


**Fig. 11.** Installation scheme of the dissipative bracing system and detail of a connection to the RC structure.

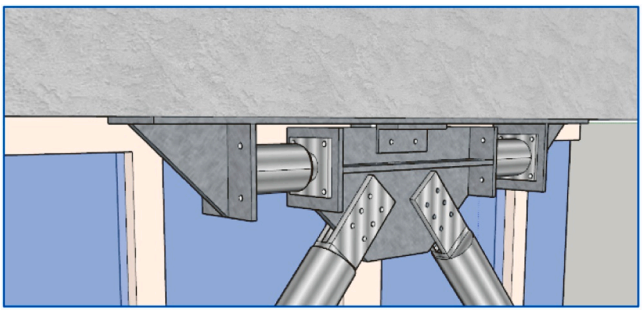

**Fig. 12.** Installation detail of a PFV damper pair.

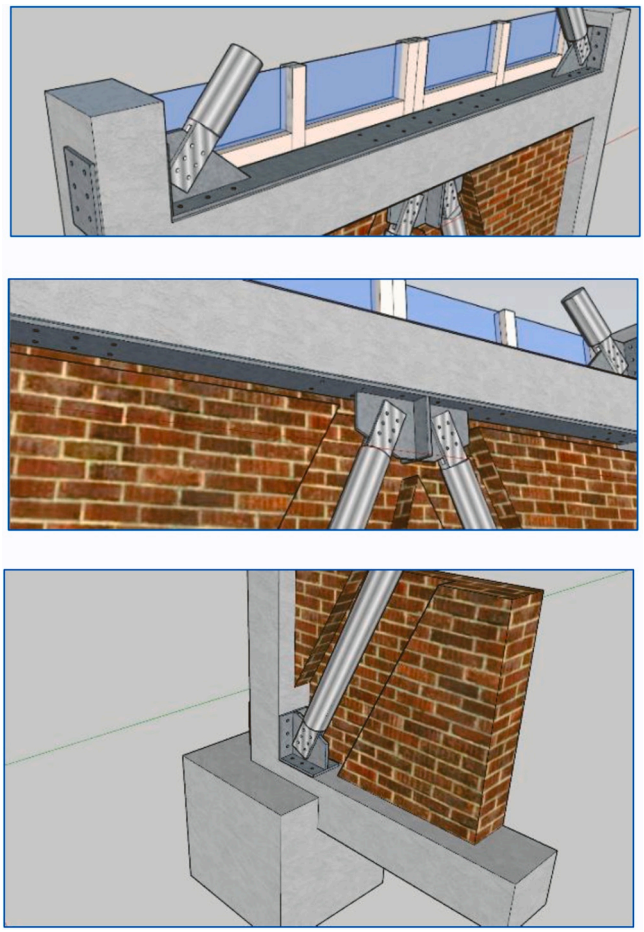

**Fig. 13.** Installation details of braces.

dissipaters are not mounted on the first level of the bracing system, where it is completed by traditional inverse-chevron shaped struts. These provide the required continuity to the system up to the foundations, while at the same time they maintain the appearance of the upper level struts. Drawings illustrating the installation details of the system are presented in Figs. 11–13, according to the general mounting scheme adopted in several early [24,25] through recent [13,26] applications of this technology by the authors. As shown in these figures, the connection plates of trusses and dampers are welded to continuous steel plates, anchored to the bottom and top faces of the RC beams by vertical steel connectors inserted in injected drillings. Trusses and dampers are bolted on site to relevant plates. Thin traces are made in the infills so as to align the centerlines of trusses with the middle plane of the masonry panels (Fig. 13). The installation works can be completely carried out outside the building, causing no downtime or interior architectural intrusion.

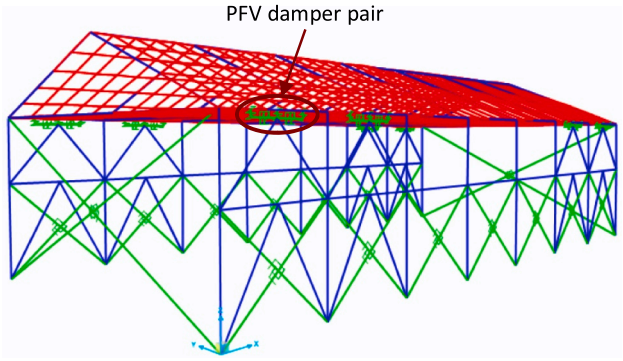


**Fig. 14.** Finite element model of the structure incorporating the dissipative bracing system.

The mechanical behaviour of the PFV devices, whose working principle is based on the flow of a pressurized highly viscous fluid through a thin annular space between piston head and tank casing, is characterized by the following damping, $F_d$, and elastic, $F_e$, force components [22,46]:

$$F_d(t) = c\,sgn[\dot{x}(t)]|\dot{x}(t)|^{\gamma} \tag{1}$$

$$F_{ne}(t) = k_2 x(t) + \frac{(k_1 - k_2)x(t)}{\left[1 + \left|\frac{k_1 x(t)}{F_0}\right|^5\right]^{1/5}} \tag{2}$$

where: $t$ = time variable; $c$ = damping coefficient; $sgn(\cdot)$ = signum function; $\dot{x}(t)$= velocity; $|\cdot|$ absolute value; $\gamma$ = fractional exponent, ranging from 0.1 to 0.2 [22]; $F_0$ = static pre-load; $k_1$, $k_2$ = stiffness of the response branches situated below and beyond $F_0$; and $x(t)$ = displacement.

The protection system was sized by referring to the BDE hazard level, using the energy-based criterion proposed in [47], governed by the following relation:

$$E_{D,\alpha DC,max} = 4(\alpha_{DC,max} - 1)V_{b,max}ID_d \tag{3}$$

where: $E_{D,\alpha DC,max}$ = energy dissipation capacity in maximum seismic response conditions tentatively assigned to the protective system, expressed as a function of the maximum demand/capacity ratio (in terms of stress states or drifts) obtained from the assessment analysis in current state, $\alpha_{DC,max}$; $V_{b,max}$ = maximum base shear calculated in current state; $ID_d$ = maximum inter-storey drift tentatively assumed in the retrofit design, coinciding with the inter-level design drift for the case study structure. By referring to (3), the sizing process was carried out by targeting a reduction factor 3 on the BDE-induced upper level drifts (which provide the most unfavorable demand/capacity ratio), so as to constrain the computed maximum $D_{wr}$ value of 2.95 % below the above-mentioned $D_{wr,LS}$ = 1 % limit. Hence, $\alpha_{DC,max}$ = 3 was assumed. Consistently, $ID_d$ was fixed at 1 % of the upper inter-level net height, i.e. $ID_d$ = 19.5 mm. Based on the $V_{b,max}$ value derived from the time-history analysis in current conditions, equal to 631 kN, the estimated energy dissipation capacity to be assigned to the protective system resulted to be as follows: $E_{D,\alpha DC,max}$ = 101 kJ.

By assuming the system be installed in the first two and last two spans of each side façade, that is, in C1-C3, C3-C5, C11-C13, C13-C15, C2-C4, C4-C6, C12-C14 and C14-C16 alignments in plan, the total number of spring-dampers to be incorporated in the dissipative braces, $n_t$, is equal to 16. By dividing $E_{D,\alpha DC,max}$ by $n_t$, the energy dissipation capacity for the maximum response cycle of each device, $E_{Ds}$, results as follows: $E_{Ds}$ = 6.3 kJ. The spring-damper type with the nearest nominal energy dissipation capacity, $E_n$, to $E_{Ds}$ has the following mechanical properties, drawn from the manufacturer's catalogue [48]: $E_n$ = 7 kJ; stroke $s_{max}$ = ± 40 mm; damping coefficient $c$ = 9.9 kN·(s/mm)$^{\gamma}$, with

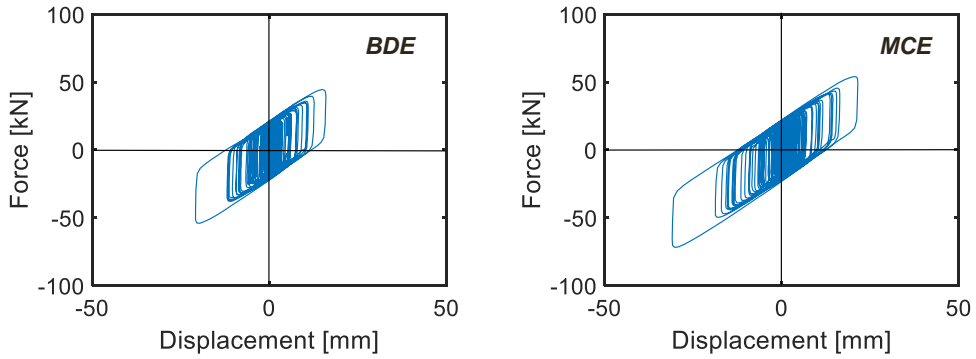


**Fig. 15.** Response cycles of the spring-damper pair highlighted in Fig. 14 obtained from the most demanding BDE and MCE-scaled groups of input accelerograms.

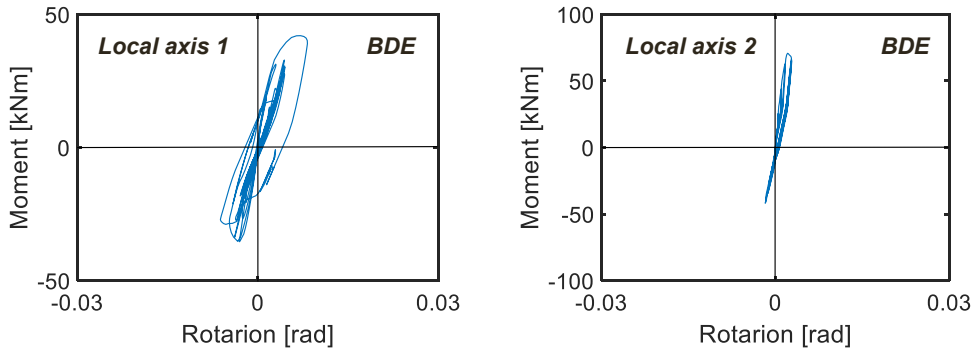


**Fig. 16.** Response cycles of the top plastic fiber hinge of column C1, around its two local axes, obtained from the most demanding BDE-scaled group of input accelerograms in retrofitted conditions.

$\gamma = 0.15$; $F_0 = 90$ kN; maximum response force $F_{max} = 150$ kN; and $k_2 = 1.74$ kN/mm. A view of the finite element model of the structure incorporating the protective system is shown in Fig. 14.

The dissipative bracing technology adopted herein causes the lateral stiffness of the retrofitted structure to increase slightly, due to the in-series dampers-to-trusses connection, and the low stiffness of the PFV dissipaters [24]. In the case study building, where the dampers are installed on the upper level only and the lower level braces are of a conventional type, the stiffening effects of the latter are nonetheless small, because of the considerable horizontal stiffness contribution by the masonry panels to the infilled level. This is reflected on the modal response in retrofitted configuration, showing very slight variations of period (from 0.364 s to 0.356 s) and EMM (from 94.9 % to 96.2 %) of the first translational mode along X, and practically no change on the first translational mode along Y (0.238 s, 96.4 %, instead of 0.24 s, 95.9 %). Period and EMM of the first rotational mode are slightly more

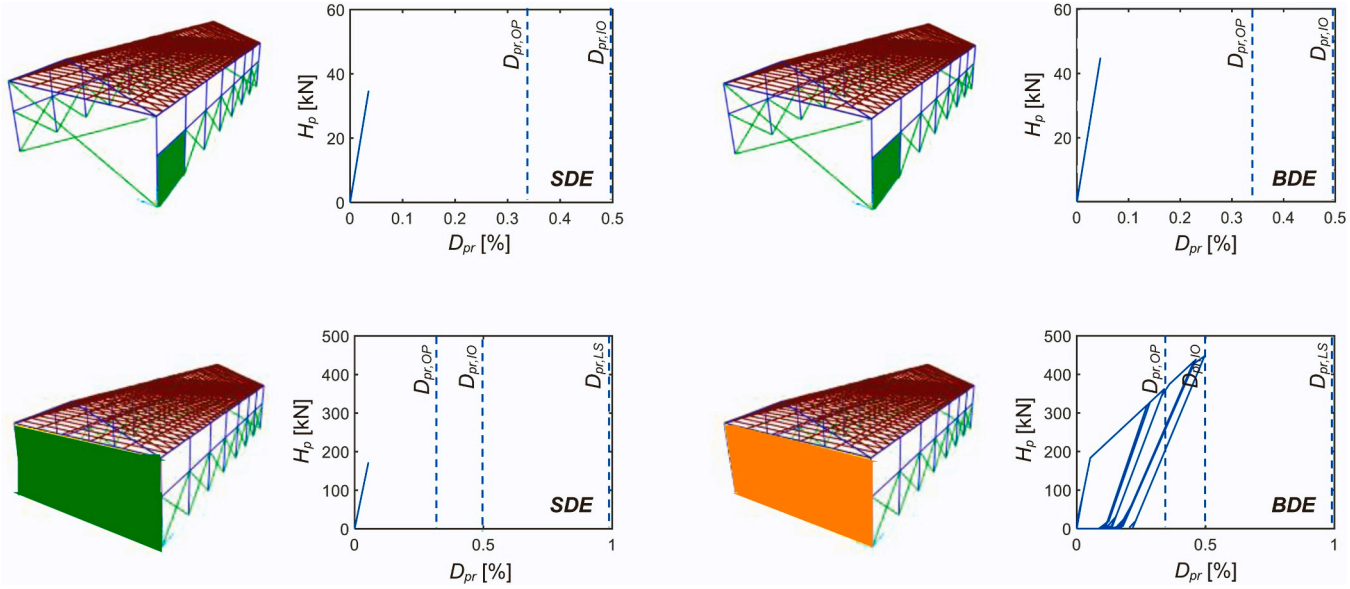


**Fig. 17.** Response cycles of a longitudinal and a transversal infill panel obtained from the most demanding SDE and BDE-scaled groups of input accelerograms, corresponding post-quake states according to the chromatic scale of the backbone curve, and reference $D_{pr,OP}$, $D_{pr,IO}$ and $D_{pr,LS}$ limits, in retrofitted conditions.

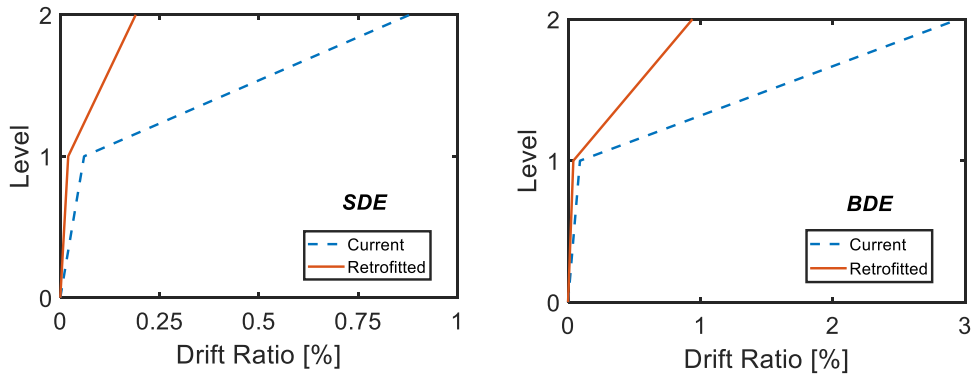


**Fig. 18.** Maximum drift ratio profiles of the building in current and retrofitted conditions.

affected, passing from 0.157 s, 73.5 % to 0.143 s, 84.6 %.

According to the Italian Standards, a first performance check was carried out on the maximum response displacements of the spring-dampers at the MCE, which resulted no greater than 32.5 mm, i.e. below the available $s_{max}$ stroke of ± 40 mm. This is visualized by the response cycles of the pair of devices highlighted by an ellipse in Fig. 14, demonstratively plotted in Fig. 15 for the most demanding group of MCE-scaled input motions. The peak damper displacement at the BDE is equal to 18.1 mm.

The post-intervention performance evaluation at the BDE yielded the following results: maximum $D_{wr}$ values of 0.94 % (corresponding to a drift of 18.4 mm, consistent with the peak damper displacement of 18.1 mm), i.e. below the $D_{wr,LS} = 1$ % limit, with a 3.14 reduction on the 2.95 % value in current state, which satisfactorily matches the $\alpha_{DC,max} = 3$ factor targeted in the sizing stage; maximum demand/capacity ratios for the second level columns equal to 1.03 in combined axial force/biaxial flexure, and 0.97 in shear, corresponding to 1.54 and 1.59 reductions, respectively; maximum demand/capacity ratios of 0.77 (flexure) and 0.68 (shear) for the top beams, with 1.56 and 1.6 decreases; peak base shear $V_{b,max} = 402$ kN, with 1.57 reduction; peak $D_{pr}$ values of 0.47 % for the terminal façades, falling in the B3 backbone curve segment, with a 1.68 decrease. As regards the SDE-related response, a $D_{wr}$ drop from 0.88 % to 0.19 % (B2 segment) is obtained. By way of example of these results, the graphs in Figs. 7 and 8 are duplicated in Figs. 16 and 17 for retrofitted conditions. As highlighted by the moment-rotation cycles around local axis 1 in Fig. 16, a minimal residual plastic demand remains at the BDE for the second level C1 column (and similarly, for the remaining columns on this level), consistently with the above-mentioned maximum 1.03 value found for the corresponding demand/capacity ratio. However, this minimal residual plastic activity, consisting of one narrow cycle for the most demanding among the seven groups of input motions, does not prompt either the implementation of an integrative local strengthening intervention on second level columns or the installation of PFV dampers with higher dissipation capacity. Fig. 17 shows the transition to the first response branch both for longitudinal and transversal panels, at the SDE, and to the first branch (longitudinal) and the third one (transversal), at the BDE. A direct comparison in terms of maximum building drift ratios in current and retrofitted conditions at the SDE and BDE is visualized in Fig. 18.

Axial force increases by no more than 10 % in the columns belonging to the vertical alignments where the dissipative bracing system is installed, due to the low stiffening effects of the latter. Consequently, no interventions are needed on these columns to improve their axial strength, as well as on relevant footings.

The post-intervention energy response time-histories, plotted in Fig. 19, point out contributions of the dissipative bracing system to the total input energy equal to about 68 % at the SDE, and 66 % at the BDE. The residual hysteretic response of columns and infills provides contributions of 1 % and 3 %, respectively. This confirms, also in terms of energy balance, the satisfactory seismic protection performance of the system.

## 5. Conclusions

The seismic assessment analyses carried out on the case study gym building confirmed a considerable vulnerability both of structural members and non-structural elements of the stock of edifices with similar characteristics built in the 1960s-1990s (including also sports halls, workshops, warehouses, archive storage facilities and manufacturing plants). This is a consequence of their special architectural layout, characterized by a RC frame structure infilled by masonry panels on the lower level of the side façades, and ribbon windows on the upper level. Indeed, this results in a seismic demand concentration on the glazed level capable of inducing severe damage, and even collapse, of windows, and notably higher stress states in columns, as compared to buildings where façades feature not sudden infill discontinuity.

The analyses in current conditions at the SDE highlighted a totally

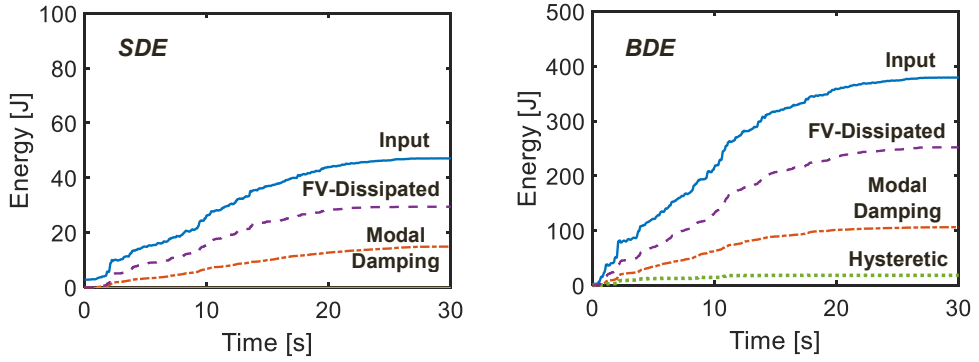


**Fig. 19.** Energy time-histories obtained from the most demanding SDE and BDE-scaled groups of input accelerograms in retrofitted conditions.

elastic response of the frame structure, and a substantially undamaged response of the infills; at the same time, peak normalized drifts of 0.88 % were found on the glazed level, i.e. neatly beyond the IO threshold for glazed curtain walls, and slightly below relevant LS limit.

The BDE-related performance evaluation pointed out unsafe conditions for the second level columns, with maximum demand/capacity ratios of 1.59 in combined axial force/biaxial flexure, as also stressed by the wide response cycles of their plastic fiber hinges, and 1.55 in shear; and for the top beams, with demand/capacity ratios of 1.2 in flexure, and 1.09 in shear. The normalized drifts of infills reached values of 0.79 % for the terminal façades, corresponding to severely damaged conditions (last branch of the backbone curve assumed to assess the response of masonry panels). The high normalized drifts computed for windows, equal to 2.95 %, bear evidence to their full collapse conditions.

The retrofit intervention proposed herein was aimed at concentrating the damping action of the dissipative bracing system on the glazed level, so as to substantially reduce its remarkable vulnerability in current state. The PFV dampers selected, pre-sized by assuming a reduction factor 3 for the glazed level drifts at the BDE, allowed reaching this target value nearly exactly, shifting normalized drifts to 0.94 %, below relevant LS-related limit.

The effects of the protective system were notably beneficial also for columns, whose drops in the stress states allowed successfully passing relevant shear checks and nearly meeting the biaxial flexure ones, as well as for the infills.

Concerning the latter, thanks to the global damping action produced by PFV devices, significant drift reductions were obtained also for the panels belonging to the front façades, oriented in orthogonal direction to the plane of installation of the dissipative braces, reducing their response below the IO drift limit of 0.5 %.

These objectives are achieved with small-sized devices and no interior architectural intrusion or interruption of building usage. This advanced retrofit solution also offers the advantage of fast installation times and pleasing appearance, prompting its future application to buildings with similar architectural and structural characteristics to the case study ones.

## CRediT authorship contribution statement

**Stefano Sorace:** Writing – review & editing, Validation, Supervision, Methodology, Investigation, Funding acquisition, Data curation, Conceptualization. **Nicola Bidoli:** Visualization, Validation, Software, Investigation, Data curation. **Gloria Terenzi:** Writing – review & editing, Validation, Methodology, Data curation, Conceptualization.

## Declaration of Competing Interest

The authors declare that they have no known competing financial interests or personal relationships that could have appeared to influence the work reported in this paper.

## Data availability

Data will be made available on request.

## Acknowledgements

The study reported in this paper was primarily funded by the Italian Department of Civil Protection within the ReLUIS-DPC Project 2022/2024, WP 15 “Normative contributions on seismic Isolation and Dissipation”, and minorly funded by the Inter-Department Project “ESPeRT” (Energy, Sustainability of Productive processes and Territorial Resilience) of the University of Udine. The authors gratefully acknowledge both financial supports.

## References

[1] Park R. A summary of results of simulated seismic load tests on reinforced concrete beam-column joints, beams and columns with substandard reinforcing details. J Earthq Eng 2002;6(2):147–74.
[2] Kam WY, Pampanin S, Elwood K. Seismic performance of reinforced concrete buildings in the 22 February Christchurch (Lyttelton) earthquake. Bull NZ Soc Earthq Eng 2011;44(4):239–78. 2011.
[3] Foti D. Shear vulnerability of old historical existing R.C. structures. Int J Archit Herit: Conserv Anal Restor 2015;9(4):453–67.
[4] Di Ludovico M, Digrisolo A, Moroni C, et al. Remarks on damage and response of school buildings after the Central Italy earthquake sequence. Bull Earthq Eng 2018;17:5679–700.
[5] Masi A, Chiauzzi L, Santarsiero G, et al. Seismic response of RC buildings during the Mw 6.0 August 24, 2016 Central Italy earthquake: the Amatrice case study. Bull Earthq Eng 2019;17:5631–54.
[6] Di Domenico M, De Risi MT, Manfredi V, et al. Modelling and seismic response analysis of Italian pre-code and low-code reinforced concrete buildings. Part II: infilled frames. J Earthq Eng 2022;27(6):1534–64.
[7] Calvi GM, Bolognini D. Seismic response of reinforced concrete frames infilled with weakly reinforced masonry panels. J Earthq Eng 2001;5(2):153–85.
[8] Stavridis A, Shing PB. Finite-element modeling of nonlinear behavior of masonry-infilled RC frames. ASCE J Struct Eng 2010;136(3):285–96.
[9] Braga F, Manfredi V, Masi A, et al. Performance of non-structural elements in RC buildings during the L'Aquila, 2009 earthquake. Bull Earthq Eng 2011;9:307–24.
[10] Baird A, Palermo A, Pampanin S. Façade damage assessment of multi-storey building in the 2011 Christchurch earthquake. Bull NZ Soc Earthq Eng 2011;44(4):368–76.
[11] Jeon J-S, Park J-H, DesRoches R. Seismic fragility of lightly reinforced concrete frames with masonry infills. Earthq Eng Struct Dyn 2015;44:1783–803.
[12] Mazza F, Donnici A. In-plane and out-of-plane seismic damage of masonry infills in existing r.c. structures: the case study of De Gasperi-Battaglia school in Norcia. Bull Earthq Eng 2021;19(1):345–76.
[13] Sorace S, Costoli I, Terenzi G. Seismic assessment and dissipative bracing retrofit-based protection of infills and partitions in RC structures. Eng Struct 2023;281:115781.
[14] Sucuoglu H, Vallabhan C. Behavior of window glass panels during earthquakes. Eng Struct 1997;19(8):685–94.
[15] Behr R. Seismic performance of architectural glass in mid-rise curtain wall. ASCE J Archit Eng 1998;4(3):94–8.
[16] Sorace S, Terenzi G. Structural assessment of a modern heritage building. Eng Struct 2013;49:743–55.
[17] Memari A, Shirazi A, Kremer P, Behr R. Seismic vulnerability evaluation of architectural glass in curtain walls. Civ Eng Archit 2014;1(2):110–28.
[18] Gorenc B, Beg D. Curtain wall façade system under lateral actions with regard to limit states. Steel Constr 2016;9(1):37–45.
[19] Caterino N, Del Zoppo M, Maddaloni G, Bonati A, Cavanna G, Occhiuzzi A. Seismic assessment and finite element modelling of glazed curtain walls. Struct Eng Mech 2017;61:77–90.
[20] Aiello C, Caterino N, Maddaloni G, Bonati A, Franco A, Occhiuzzi A. Experimental and numerical investigation of cyclic response of a glass curtain wall for seismic performance assessment. Constr Build Mater 2018;187:596–609.
[21] Gandelli E, Pertica G, Facconi L, Minelli F, Preti M. Seismic retrofit of warehouses with masonry infills and glazed curtain walls through hysteretic braces: refinement of the Italian Building Code provisions. Appl Sci 2023;13(15):8634.
[22] Sorace S, Terenzi G. Non-linear dynamic modelling and design procedure of FV spring-dampers for base isolation. Eng Struct 2001;23:1556–67.
[23] Terenzi G, Costoli I, Sorace S. Activation control extension of a design method of fluid viscous dissipative bracing systems. Bull Earthq Eng 2020;18(8):4017–38.
[24] Sorace S, Terenzi G. Seismic protection of frame structures by fluid viscous damped braces. ASCE J Struct Eng 2008;134:45–55.
[25] Sorace S, Terenzi G, Fadi F. Shaking table and numerical seismic performance evaluation of a fluid viscous-dissipative bracing system. Earthq Spectra 2012;28:1619–42.
[26] Terenzi G, Fuso E, Sorace S. Structural performance study and improvement of Artemio Franchi Stadium in Florence. Eng Struct 2024;298:115969.
[27] Law 5 November 1971. Technical Standards for the regulation of normal and prestressed reinforced concrete and steel structures. Rome (Italy): Italian Republic, GU no. 321–1971 [in Italian].
[28] Ministerial Decree 30 May 1972. Implementing Decree of the Technical Standards for the regulation of normal and prestressed reinforced concrete and steel structures. Rome (Italy): Italian Republic, GU no. 190–1972 [in Italian].
[29] Ministerial Decree 3 March 1975. Technical Standards for structures in seismic zones. Rome (Italy): Italian Republic, GU no. 93–1975 [in Italian].
[30] Ministerial Decree 17 January 2018. Update of Technical Standards for constructions. Rome (Italy): Italian Ministry of Infrastructure and Transport, GU no. 42–2018 [in Italian].
[31] Circular 21 January 2019 no. 7. Instructions for the application of the Update of Technical Standards for constructions. Rome (Italy): Ministry of Infrastructure and Transport, Ordinary supplement to G.U. no. 35–2019 [in Italian].
[32] CSI. SAP2000NL. Theoretical and user's manual. Release 25.09. Berkeley, CA, USA: Computers & Structures Inc.; 2024.
[33] Stafford Smith B. Behaviour of square infilled frames. ASCE J Struct Div 1966;92(1):381–403.

[34] Bertholdi SH, Decanini LD, Gavarini C. Telai tamponati soggetti ad azione sismica, un modello semplificato: confronto sperimentale e numerico. Proceedings of the VI Italian National Conference on Earthquake Engineering 1993;2:815–24.
[35] Crisafulli FJ, Carr AJ, Park R. Analytical modelling of infilled frame structures—a general overview. Bull NZ Soc Earthq Eng 2000;33(1):30–47.
[36] Morandi P, Hak S, Magenes G. Performance-based interpretation of in-plane cyclic tests on RC frames with strong masonry infills. Eng Struct 2018;156:503–22.
[37] Mazza F. In-plane–out-of-plane non-linear model of masonry infills in the seismic analysis of r.c. framed buildings. Earthq Eng Struct Dyn 2019;48(4):432–53.
[38] Mucedero G, Perrone D, Brunesi E, Monteiro R. Numerical modelling and validation of the response of masonry infilled RC frames using experimental testing results. Buildings 2021;10(10):182.
[39] Gaetani d'Aragona M, Polese M, Prota A. Effect of masonry infill constitutive law on the global response of infilled RC buildings. Buildings 2021;11(2):57.
[40] Dias-Oliveira J, Rodrigues H, Asteris PG, Varum H. On the seismic behavior of masonry infilled frame structures. Buildings 2022;12(8):1146.
[41] JASS14. Japanese architectural Standard specification for curtain walls. Minato-ku, Tokyo, Japan: Architectural Institute of Japan (AIJ); 1996.
[42] JGJ102. Ministry of housing and urban-rural of the People's Republic of China (MOHURD). Technical code for glass curtain wall engineering. Beijing: China Architecture & Building Press; 2003 (in Chinese).
[43] CSA-S832. Standard for seismic risk reduction of operational and functional components (OFCs) of buildings. Rexdale, Ontario, Canada: Canadian Standards Association; 2006.
[44] FEMA E-74. Reducing the risks of nonstructural earthquake damage – a practical guide. Washington, D.C., USA: Federal Emergency Management Agency; 2011.
[45] ASTM C 1048. Standard specification for heat-strengthened and fully tempered flat glass. West Conshohocken, PA, USA: American Society for Testing and Materials (ASTM); 2012.
[46] Pekcan G, Mander JB, Chen SS. The seismic response of a 1:3 scale model R.C. structure with elastomeric spring dampers. Earthq Spectra 1995;11:249–67.
[47] Terenzi G. Energy-based design criterion of dissipative bracing systems for seismic retrofit of framed structures. Appl Sci 2018;8(2):268.
[48] Dyna Shock System. URL ⟨http://www.dynashocksystem.com/⟩; accessed 13 May 2023.